

RESEARCH ARTICLE | AUGUST 24 2022

Spatial correlations and relative velocities of polydisperse droplets in homogeneous isotropic turbulence

Hangyu Zhu (朱航宇) ; Chong Pan (潘翀) ; Huan Lian (连欢) ✉



Physics of Fluids 34, 083320 (2022)

<https://doi.org/10.1063/5.0101945>



View
Online



Export
Citation

CrossMark

Articles You May Be Interested In

Impact analysis of SVC on stepped distance protection modeling and simulation using PSCAD/EMTDC

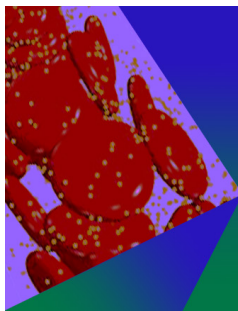
AIP Conference Proceedings (September 2022)

Comparative study of the effects of SVC and TCSC on the small signal stability of a power system with renewables

Journal of Renewable and Sustainable Energy (June 2019)

SVC compensated transmission line protection using wavelet approach

AIP Conference Proceedings (May 2022)



Physics of Fluids

Special Topic: Flow and Forensics

Submit Today!

Spatial correlations and relative velocities of polydisperse droplets in homogeneous isotropic turbulence

Cite as: Phys. Fluids **34**, 083320 (2022); doi: 10.1063/5.0101945

Submitted: 5 June 2022 · Accepted: 25 July 2022 ·

Published Online: 24 August 2022






View Online



Export Citation



CrossMark

Hangyu Zhu (朱航宇),^{1,2,3}  Chong Pan (潘翀),^{2,4}  and Huan Lian (连欢)^{1,a)} 

AFFILIATIONS

¹State Key Laboratory of High Temperature Gas Dynamics, Institute of Mechanics, Chinese Academy of Sciences, Beijing 100190, China

²Fluid Mechanics Key Laboratory of Education Ministry, Beihang University, Beijing 100191, China

³Department of Mechanics and Aerospace Engineering, Southern University of Science and Technology, Shenzhen 518055, China

⁴Aircraft and Propulsion Laboratory, Ningbo Institute of Technology, Beihang University, Ningbo 315800, China

^{a)} Author to whom correspondence should be addressed: hlian@imech.ac.cn

ABSTRACT

We investigate the motions of polydisperse droplets in homogeneous and isotropic turbulence at Reynolds numbers $Re_\lambda = 200\text{--}300$. The emphasis is put on the parameter dependences of spatial velocity correlations (SVCs) and relative velocities (RVs) of droplets, which are relevant to particle transport and dispersion in turbulence and have been less studied in experiments. The Kolmogorov-scale Stokes number is $St_p = 10^{-1}\text{--}10^1$, and the settling parameter, i.e., the ratio of particle settling velocity to fluid velocity fluctuations, is $Sv_L = 0.5\text{--}2.0$. Using high-resolution measurements, we can resolve the motions of turbulence and droplet over a wide range of scales ($10^{-1}\eta$ to $10^2\eta$, η is Kolmogorov length). The parabolic behavior in droplet SVCs near the origin is observed, similar to turbulence. The droplet SVCs are smaller than turbulence for all scales and decrease with both St_p and Sv_L . At large scales, the droplet RVs, smaller than those of turbulence due to the inertial filtering effect, also decrease with St_p and Sv_L . At small scales, the path-history effect leads to larger droplet RVs than fluid RVs. Interestingly, we find RVs present a non-monotonic trend with St_p and reach a valley at $St_p \approx 1.0$. It may originate from particle clustering and preferential sweeping effects, which both prevail at $St_p \approx 1.0$. It is also found that droplet motions are less intermittent than turbulence. This is in contrast to the previous observations by simulations with the gravity effect being ignored. The intermittency of droplet RVs decreases with Sv_L due to the diminished droplet-turbulence interactions, and it presents opposite trends with St_p for small and large scales. Finally, the balance between the effects of path histories and turbulent structures makes the velocity statistics of droplets quasi-independent from the scale in the range of the dissipative scale ($r \lesssim 5\eta$).

Published under an exclusive license by AIP Publishing. <https://doi.org/10.1063/5.0101945>

I. INTRODUCTION

Particle-laden turbulent flows are widely encountered in many environmental and engineering situations, including pollutant distribution, atmosphere clouds, and spray combustion. Inertial particles dispersed in turbulence present profoundly different dynamics from fluid particles. This complex physical process has attracted much attention from researchers in fluid mechanics.^{1–3}

Turbulent coherent structures affect the motions of finite-size particles to some degree; namely, the kinematics of particle motions present spatial coherency over a finite length scale range. This can be quantified by the spatial velocity correlations (SVCs), defined as the ensemble-averaged velocity products of the two measured points

divided by square of velocity fluctuation intensity. According to Février *et al.*,⁴ SVC is made up of two contributions: spatially correlated motion due to the underlying turbulent structures and random uncorrelated motion rooted in particle inertia or particle memory of interactions with distant eddies.

Février *et al.*⁴ found that at small separations r , the SVCs decreased appreciably with the increase in particle inertia, and this was experimentally confirmed in a turbulent vertical channel flow by Fong *et al.*⁵ This framework was then employed in many simulations to analyze different particle-laden flows.^{6,7} However, there have been few experimental investigations examining particle SVCs; Khalitov and Longmire,⁸ Fong *et al.*,⁵ and Sahu *et al.*⁹ are the notable examples, but

none of these considered homogeneous and isotropic turbulence (HIT). Moreover, a discontinuity has been noticed in the SVCs at the origin.^{4,6,10} Nonetheless, the particle SVCs near the dissipative range have rarely been examined, especially in experiments. The SVC function in the dissipative range of HIT presents a parabolic form,¹¹ but it remains unclear whether this behavior is also shown for inertial particles.

Another interesting topic is the collision between neighboring particles. The collision rate is strongly related to both the local concentration and the relative velocity (RV).^{12,13} The latter is defined as the velocity difference between two particles. For two inertial particles that are very close with each other (i.e., with small r), RVs can be rather large, resulting in a higher probability of collisions. For large separation, RVs have important implications for the relative dispersion of particles in turbulence.¹⁴ The RVs of particles are determined by three mechanisms: preferential concentration, path histories, and inertial filtering. These effects are associated with several important parameters, including the particle Stokes number St_p , i.e., the ratio of the particle relaxation time to the Kolmogorov timescale, and the settling parameter Sv , i.e., the ratio of particle settling velocity to the characteristic velocity of turbulence. For $St_p \ll 1.0$, preferential concentration, which describes that inertial particles accumulate in the region of low-vorticity and high-strain,¹⁵ dominates and reduces the particle RVs.¹⁶ The path-history effect, i.e., inertial particles retaining a finite memory of the fluid RVs that they have experienced along their path history, becomes dominant for $St_p \gtrsim 1.0$ and increases the RVs at small separations.^{17,18} At large separations, the inertial filtering effect, i.e., the tendency of inertial particles to filter out high frequency velocity fluctuations of the turbulent field, is regarded to be the dominate effect to reduce particle RVs.^{16,19–22}

Previous studies on particle RVs and their parameter dependences have overwhelmingly involved numerical simulations. It seems undisputed that at large scales, the particle RVs decrease with the increase in St_p due to inertial filtering;^{16,18–20} however, at small scales, there is less consensus. Near the dissipative range, some studies have found that particle RVs increase with St_p without the effect of gravity.^{14,16,20} However, Pan and Padoan²³ found that the RVs peaked at $St_p \approx 10$ for identical particles, while for bidisperse particles, they reach a minimum when $St_p < 7$. Moreover, the effect of gravity complicates this picture. Ireland *et al.*²² found that the inclusion of gravity reduced the RVs for all separations, and the RVs were found to be smallest for $St_p \sim 1.0$ when Sv is large.

To the best of our knowledge, the only experimental observations of the St_p dependence of particle RVs have been by Saw *et al.*²⁴ and Dou *et al.*²⁵ In an enclosed turbulence chamber, Saw *et al.* found that, near the dissipation range, the particle RVs increased with St_p over a small range of St_p (0.05–0.50). Dou *et al.* also observed this trend, although their measurements exhibited relatively large errors for $St_p \gtrsim 1.0$. Moreover, most numerical simulations have not considered particle–particle interactions, although Bragg *et al.*'s study²⁶ is a notable exception. However, inspired by the experiments of Yavuz *et al.*,²⁷ Hammond and Meng²⁸ found experimentally that particle–particle interactions, including hydrodynamic interactions, lead to a remarkable enhancement of the RVs at small separations. Therefore, more reliable information relating to the effect of St_p on the RVs is needed, especially for $St_p \gtrsim 1.0$ and $r/\eta \lesssim 1.0$. In addition, although previous numerical simulations have suggested the effects of settling on particle

motion, the variation of the RVs with Sv has not yet been experimentally investigated.

The intermittency of the particle RVs, measured by the flatness of the RV distributions, is of significance because it relates to extreme events, which play a key role in inter-particle collision and dispersion. However, the dependences of the parameters (e.g., St_p and Sv) on intermittency in both the small- and large-scale ranges have not been fully addressed. Using direct numerical simulation (DNS) and ignoring gravity, Bec *et al.*¹⁴ and Salazar and Collins²⁰ demonstrated that the intermittency of the RVs of inertial particles is much stronger than that of the RVs of turbulence, and it increases with St_p . However, recent simulations^{22,29} have suggested that the inertial-particle RV intermittency is noticeably weakened by gravity. The experiments by Saw *et al.*²⁴ represent the only such investigation. They found that the intermittency of particle motion near the dissipative range became higher with decreasing scale and increasing St_p (< 0.5).

This brief review of the literature shows that there are many important factors that have been neglected in most previous simulations; furthermore, these factors could have significant impacts on the motion of particles in turbulence and may not be avoidable in natural phenomena. These factors include polydispersity,^{30,31} gravity,^{22,32–35} and particle–particle interactions.^{27,28} As such, experimental investigations are needed to establish whether the observations from simulations are applicable under more complex circumstances. Furthermore, the responses of inertial particles to fine-scale ($\sim \eta$) and large-scale ($\sim 10^2 \eta$) turbulent structures are different. However, in both simulations and experiments, there has been relatively little systematic exploration of inertial particles' responses to turbulent motions over a broad range of length scales. With this background, we conducted experiments to investigate the RVs and SVCs of droplets in HIT over a wide scale range ($10^{-1} \eta$ to $10^2 \eta$) and explored their St_p and Sv_L dependences. We also considered the effects of gravity by comparing relevant statistics between the gravity and horizontal directions.

The remainder of this paper is structured as follows. The experimental setup and measurement technique are introduced in Sec. II. Sections III and IV present the SVCs and RVs of droplets, respectively. The effects of St_p and Sv_L and their corresponding physical mechanisms are discussed in detail. The results for single-phase turbulence are also shown for comparison. Concluding remarks are given in Sec. V.

II. EXPERIMENTAL SETUP

Zero-mean-flow HIT can be generated by an open chamber configuration referred to as a “turbulence box,” which features multiple woofers or fans pointing toward a central point.^{36,37} In these experiments, the turbulence box consisted of eight woofers, which were each covered by a perforated rectifier board with 50 small holes. These were mounted on a cubic frame to produce eight air-jet arrays, as shown in Fig. 1. In this system, adjusting the excitation voltages of the independent woofers can adjust the air-jet intensities and achieve HIT flow in the center of the cubic frame. The resulting HIT domain has a size of approximately $50 \times 50 \times 50 \text{ mm}^3$. This turbulence box, configured in a laboratory of the Institute of Mechanics at the Chinese Academy of Sciences, is conducive to the dispersion of gas-phase tracer particles and discrete particles in two-phase flow measurements. More information about the facility can be found in the report of Lian *et al.*³⁸

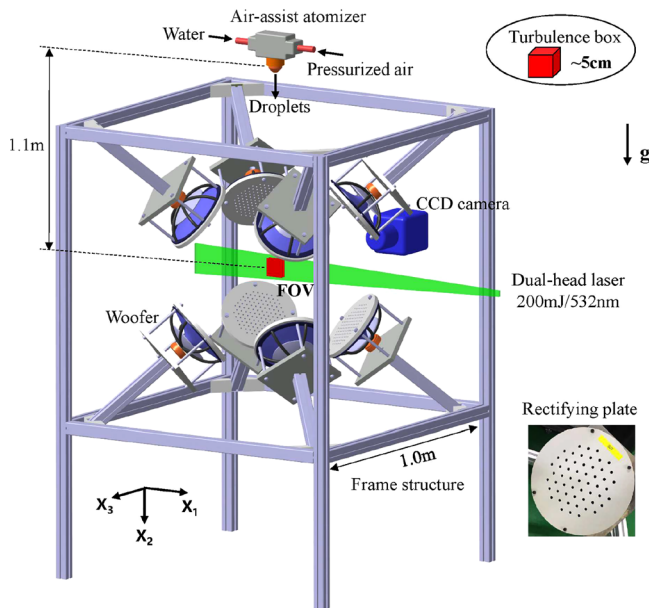


FIG. 1. Schematic diagram of the measurement system for the droplet-laden HIT experiments, including the turbulence-generation device, air-assist atomizer, PIV measurement configuration, and definition of coordinates.

A. Turbulence characterization

We used a particle image velocimetry (PIV) system to obtain the characteristics of the HIT region; the measurement and calculation parameters are summarized in Table I. For these measurements, the air flow was seeded with 3- μm organic oil drops as tracer particles produced by a high-temperature particle generator. The beam from a dual-head Nd:YAG laser with a wavelength of 532 nm and a maximum energy of 200 mJ/pulse was passed through a carefully designed lens group to form a laser sheet with a thickness of approximately 1 mm. A double-exposure ultra-high-resolution CCD camera (IMPERX ICL-B6640, 12 bit) with a sensor size of 4400×4400 pixels was equipped with a 180-mm lens to capture the particles in the measurement domain with a digital image resolution of $12 \mu\text{m}/\text{pixel}$. The sampling frequency was 1 Hz, and 1800 uncorrelated realizations for each case were recorded. A state-of-the-art cross correlation algorithm

TABLE I. Measurement and PIV-calculation parameters for HIT.

Parameter	Value
Sampling frequency	1 Hz
Camera sensor size	4400×4400 pixels
Field of view (FOV)	$53.5 \times 53.5 \text{ mm}^2$
Digital image resolution	$12 \mu\text{m}/\text{pixel}$
Sampling number	1800
Final interrogation window	32×32 pixels
Overlap ratio	75%
PIV spatial resolution	0.42 mm ($2\eta/\text{vector}$)
PIV vector spacing	0.1 mm (0.5η)

with window deformation and multi-resolution iteration was used for the velocity-field calculations. The interrogation window of the final pass was 32×32 pixels with an overlap ratio of 75%. Therefore, the spatial resolution of the velocity field was 0.42 mm ($\sim 2.0\eta$, where η is the Kolmogorov length scale) with a vector spacing of 0.1 mm ($\sim 0.5\eta$), which is typically considered appropriate for capturing fine-scale turbulence without significant bias.

As illustrated in Fig. 1, the horizontal direction x_1 and gravity direction x_2 are defined in the measurement plane, and the corresponding velocity components are u_1 and u_2 , respectively. The subscript “rms” is used to denote the corresponding root-mean-squared fluctuation intensities, and the subscripts f and p denote variables of the fluid and discrete phases, respectively. The present experiments explored two Re_λ cases by adjusting the input voltages of the woofers. The Reynolds number Re_λ can be defined as $Re_\lambda = \lambda_T(k/3)^{1/2}/\nu$, where the turbulent kinetic energy can be calculated with $k = 3(u_{f1,rms}^2 + u_{f2,rms}^2)/2$ and ν is kinematic viscosity. The transverse Taylor microscale is estimated with

$$\lambda_T = (5\nu k/\epsilon)^{1/2}, \tag{1}$$

where ϵ is the energy dissipation rate and estimated with

$$\epsilon = 4\nu \left[\left\langle \left(\frac{\partial u_1}{\partial x_1} \right)^2 \right\rangle + \left\langle \left(\frac{\partial u_2}{\partial x_2} \right)^2 \right\rangle + \left\langle \left(\frac{\partial u_1}{\partial x_1} \frac{\partial u_2}{\partial x_2} \right) \right\rangle + \frac{3}{4} \left\langle \left(\frac{\partial u_1}{\partial x_2} \frac{\partial u_2}{\partial x_1} \right)^2 \right\rangle \right]. \tag{2}$$

The basic parameters of the HIT for these two Re_λ are summarized in Table II. In the Appendix, we present the verification of the homogeneity and isotropy of these turbulent flows.

Figure 2 shows the SVC of the fluid phase, which is calculated using

$$\rho_{ij}(r_j, \mathbf{x}) = \langle u_i(\mathbf{x}, t) u_j(\mathbf{x} + r_j, t) \rangle / u_{i,rms}^2, \tag{3}$$

where the subscript i indicates the velocity components and j denotes the x_1 or x_2 directions; when $i = j$, ρ_{ij} denotes the longitudinal correlation function; when $i \neq j$, ρ_{ij} denotes the transverse correlation function; the angle brackets $\langle \rangle$ denote the ensemble average; \mathbf{x} is the position of a fluid parcel; and r_j is the separation between two points

TABLE II. Basic parameters of HIT.

Parameter	Units	Case a	Case b
Reynolds number (Re_λ)	...	227	264
Kinematic viscosity (ν)	$10^5 \text{ m}^2/\text{s}$	1.57	1.57
Turbulent kinetic energy (k)	m^2/s^2	0.85	1.15
Turbulent intensity ($u_{f,rms}$)	m/s	0.75	0.88
Intensity ratio ($u_{f1,rms}/u_{f2,rms}$)	...	1.03	1.02
Energy dissipation rate (ϵ)	m^2/s^3	1.48	2.02
Kolmogorov length (η)	μm	226	209
Kolmogorov time (τ_η)	ms	3.3	2.8
Kolmogorov velocity (u_η)	m/s	0.068	0.075
Taylor microscale (λ_T)	mm	6.71	6.68

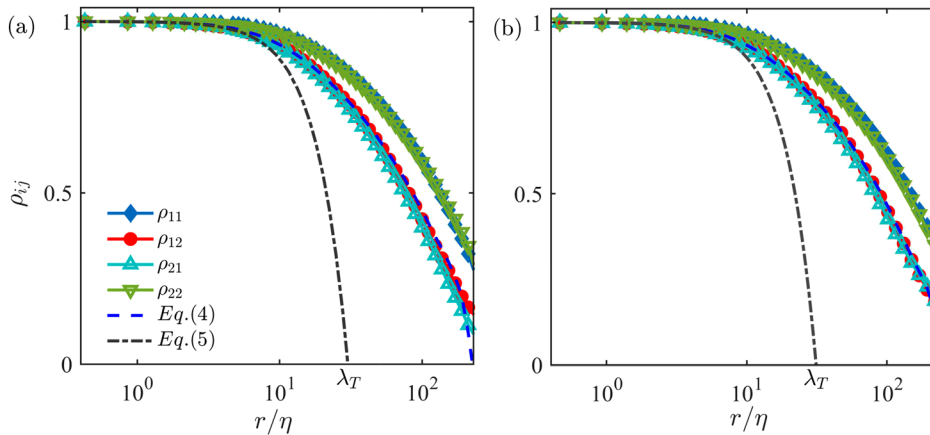


FIG. 2. SVC of fluid phase: (a) $Re_\lambda = 227$, $\lambda_T \approx 30.1\eta$ (6.80 mm); (b) $Re_\lambda = 264$, $\lambda_T \approx 31.4\eta$ (6.56 mm). The theoretical result of ρ_{21} deduced from Eq. (4) is also presented as the blue dashed line for comparison. The dash-dotted parabolic curve for Eq. (5) is deduced from the parabolic behavior of ρ_{12} (or ρ_{21}) near $r=0$, and λ_T is the intersection of this curve with the r axis.

in the x_j direction. We can observe that both $\rho_{11} = \rho_{22}$ and $\rho_{12} = \rho_{21}$ are fairly well satisfied for $r/\eta = 10^{-1}$ to 10^2 . The theoretical result of ρ_{21} under isotropic conditions based on the relation³⁹

$$\rho_{ij} = \rho_{ii} + \frac{r}{2} \frac{\partial \rho_{ii}}{\partial r} \quad (4)$$

is also shown as the blue curve, and this collapses well onto the plot of ρ_{21} calculated from the velocity field. We also calculated the longitudinal and transverse integral length scales of the turbulence and found that $L_{ii}/L_{jj} \approx 1.02$ and $L_{ii}/L_{ij} \approx 1.85$ ($i \neq j$). Within the range of experimental uncertainty, these observations indicate that the turbulent flows are isotropic.^{36,37,40}

Fitting a parabola near the origin of the SVC function is a common way to determine λ_T if one can resolve scales much smaller than it. Thanks to the high spatial resolution of this experiment, this parabolic behavior can be observed in Fig. 2. The value of λ_T can, thus, be obtained from the second-order derivative of the parabolic curve ρ_{ij} at $r=0$,³⁹ i.e.,

$$\rho_{ij} = 1 - (r/\eta)^2 / \lambda_T^2 \quad (i \neq j), \quad (5)$$

$$\lambda_T^2 = - \frac{2}{\partial^2 \rho_{ij} / \partial r^2 |_{r=0}}. \quad (6)$$

The values of λ_T obtained from Eqs. (5) and (6) are very close to those obtained from Eq. (1) listed in Table II. This indicates the reasonability and robustness of this high-resolution data.

B. Droplet injection and characterization

The polydisperse droplets were produced by an air-assist atomizer placed 1.1 m above the HIT domain, as shown in Fig. 1. The droplet sizes and volume fractions were controlled by adjusting the inlet water-flow rate and air pressure at the atomizer. More information concerning the atomizer can be found in the report of Lian *et al.*³⁸ It is noted that the velocity fields of the discrete phase (droplets) and continuous phase (turbulence) were measured separately in these experiments. This is because it is difficult to distinguish droplets from tracer particles in PIV images using their brightness or pixel size. Therefore, when measuring the motions of droplets in two-phase turbulence, we turned on the woofers but did not release the tracer particles.

Nevertheless, for all two-phase flows in this study, the particle volume fraction Φ_V was approximately 5×10^{-6} , which is close to the one-way coupled regime,⁴¹ indicating that the droplet motion will have had only a small effect on the turbulent flows.

We varied the features of the droplets by adjusting the air pressure in the atomizer with the water-flow rate unchanged. A laser particle-size analyzer (LPSA; Bettersize2000S) was used to measure the size distributions of droplets in the measurement domain. For the different cases, the Sauter mean diameter D_{32} of the droplets, defined as the ratio of the droplet volume to droplet surface area, varied slightly between 35 and 40 μm , and the droplet size had a wide spread of $d_p = 10$ to 120 μm , which are much smaller than the Kolmogorov scale η (see Table II); in other words, the droplet size distribution was in a polydisperse regime, as shown in Fig. 3. The droplet sizes in droplet images can be obtained with the following process. The droplet images were binarized by setting a brightness threshold and obtained many connected regions with high brightness occupied by droplets shown in Fig. 3(a). Then, the pixel sizes (d_{pix}) of the connected regions (i.e., droplets) can be calculated. In Fig. 3(b), we show the probability density functions (PDFs) and cumulative distribution functions (CDFs) of droplet pixel sizes for two cases. The two density functions can be defined as $P(a < \zeta < b) = \int_a^b PDF(t) dt$ and $CDF(\zeta) = \int_{-\infty}^{\zeta} PDF(t) dt$, where P is the probability for $a < \zeta < b$ and ζ can be d_{pix} or d_p . The physical size distributions of droplets are shown in Fig. 3(c). As the shapes of these two distributions are close to a lognormal distribution,^{42,43} one can roughly convert the pixel sizes in the droplet images to their physical sizes.

The particle Stokes number St_p is defined as τ_p / τ_η , where τ_η is the Kolmogorov timescale of turbulence (see Table II). The particle relaxation time τ_p can be calculated from $\tau_p = \rho_p d_p^2 / 18 \nu \rho_f (1 + 0.15 Re_p^{0.687})$,^{44,45} where the density ratio of the two phases is $\rho_p / \rho_f \approx 775$; the particle Reynolds number based on the slip velocity u_r was estimated to be $Re_p = d_p u_r / \nu \approx 1.0$. Accordingly, the St_p of the droplets in the turbulence spans the range 10^{-1} to 10^1 [see Fig. 3(c)] and its mean value is in the range 0.95–1.25 based on D_{32} .

The importance of the settling of particles in turbulence can be characterized by the settling parameter,^{33,46} which is defined as the ratio of the settling velocity of the particles to the characteristic velocity of the turbulence. Both the small-scale energetic motions and large-scale structures in the turbulence are consequential in determining the particle motion. Therefore, two different settling parameters are

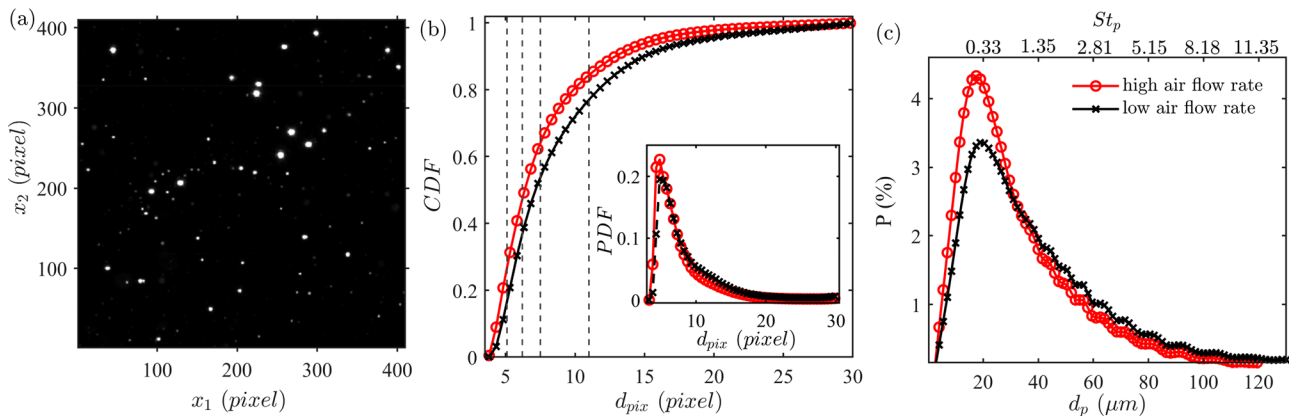


FIG. 3. (a) Zoomed snapshot of a droplet image showing polydispersity and (b) CDFs and (inset) their corresponding PDFs of the pixel sizes of droplets d_{pix} deduced from the images for two air-flow rates in the atomizer. The four dashed lines divide the ensemble into five parts; in each of these parts, the number of sampled droplets accounts for approximately 20% of the total and is of the order of 10^6 . (c) Physical size distributions of droplets measured by LPSA in the measurement domain for two air flow rates in the atomizer.

defined as follows: $Sv_L = \bar{u}_{p2}/u_{f,rms}$ and $Sv_\eta = \bar{u}_{p2}/u_\eta$, where u_η is the Kolmogorov turbulence velocity (Table II) and \bar{u}_{p2} is the mean settling velocity of the droplets. The droplet velocity was calculated using an in-house-developed hybrid particle tracking/particle image velocimetry algorithm. This algorithm can eliminate the pixel-lock effect and minimize contamination from inaccurate droplet-center identification. The uncertainty of droplet matching was estimated to be approximately 0.1 pixel, which is consistent with that in the PIV calculations. More information about this algorithm can be found in the report by Zhu *et al.*⁴⁷ The parameters of the droplets are listed in Table III. The dimensionless parameter $T_d = t_d/\tau_\eta$ is defined as the time t_d normalized by τ_η taken for the drops to pass vertically through the turbulence box. For all tested cases, $T_d > 13$, indicating that the fine-scale turbulent motions can have an impact on the falling droplets.

The involved parameters here are St_p , Sv_L (or Sv_η), and Re_λ . However, these parameters are in reality not decoupled, and it is not feasible to vary only one parameter at a time in a laboratory study, as noted in previous reports.^{42,46} Droplets of different sizes have different settling velocities (Sv_L) and different degrees of response (St_p) to turbulent flows of different scales. The effect of Re_λ on droplet motion is not the focus of this work, but two similar Re_λ values (with a difference of 15%) were used to verify the repeatability of relevant results. The Sv_L dependence of droplet motion will be investigated by considering the velocity statistics in four cases (with similar St_p distributions), while the St_p dependence will be discussed using conditional statistics based on the droplet sizes in each Sv_L case. As shown in Fig. 3(b), for each Sv_L , we divided the droplet samplings into five parts according to

TABLE III. Basic parameters of droplets for four tested cases.

Parameter	Case 1	Case 2	Case 3	Case 4
Sv_L	0.58	0.85	1.15	1.60
Sv_η	6.8	10.0	12.6	17.6
T_d	37.8	25.8	19.0	13.6

their sizes (or St_p), in each of which the number of samples accounts for approximately 20% of the total and is of the order of 10^6 .

III. DROPLET SVCs

We first consider SVCs to provide information about the degree of spatial coherency of the droplet motion. Particle SVCs have been experimentally investigated in channel flows^{5,8} and polydisperse sprays.⁹ Due to the discrete nature of the droplet velocity data, the calculation of the SVCs for the droplet phase using Eq. (3) is more complicated than that for the fluid phase. We divided the field of view (FOV) into many x_1 -direction bins with a width of the minimum resolved scale of the present turbulence data (0.5η ; r_2 is thus very small). We then categorized $u_{pi}(x)u_{pi}(x+r_1)$ for every pair of droplets using r_1 with an interval of 0.5η and ensemble-averaged them in each bin. Their normalization by $u_{pi,rms}^2$ results in ρ_{i1} . Similarly, we obtained ρ_{i2} by dividing the FOV into many x_2 -direction bins and ensemble-averaging $u_{pi}(x)u_{pi}(x+r_2)$ according to r_2 .

Figure 4 shows the SVCs (ρ_{ij}) for all tested cases of the two phases. These plots lead to several interesting observations. First, the ρ_{ij} plots for the droplet phase are found to be very similar in shape to those of the fluid phase, but the values are relatively smaller, especially at smaller scales. In particular, there is a gap between unity and ρ_{ij} at the origin, which is consistent with the results of previous numerical studies.^{4,10} According to Février *et al.*,⁴ the particle velocity consists of a contribution from the underlying turbulent flows and a spatially random uncorrelated motion component rooted in particle inertia. This gap is, thus, a measure of the fraction of random uncorrelated motion.^{4,5}

Second, in the dissipation range ($r \approx \eta$), the ρ_{ij} plots for droplets also unexpectedly present a parabolic form similar to that seen in turbulent flows, which was not observed in previous studies and may be important for the numerical models.^{4,10} At small separations, the droplet motion is dominated by the path-history mechanism in which the inertial particle pairs reserve a finite memory of turbulent velocity fluctuations they have experienced along their path history.⁵⁰ Specifically, the droplet motions are inherited from the coherence of small-scale turbulent motions, but they are less coherent due to inertial effects.

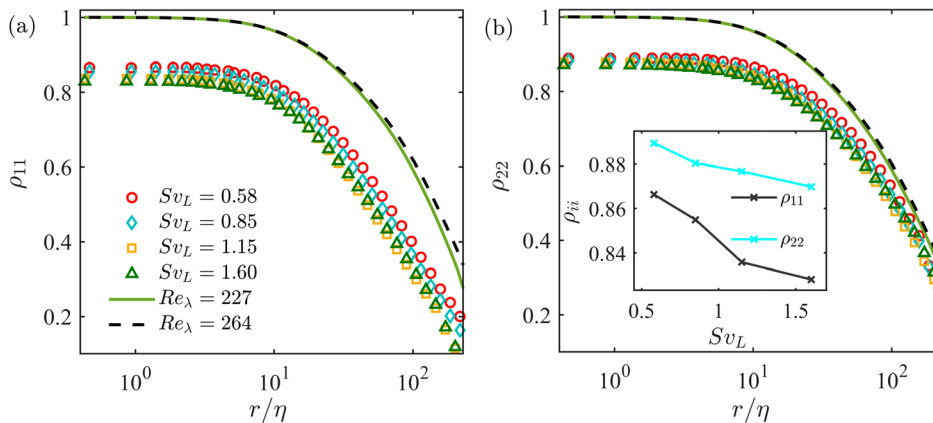


FIG. 4. Longitudinal SVCs of droplet and fluid phases: (a) ρ_{11} ; (b) ρ_{22} . The inset of (b) shows the correlation coefficients as functions of Sv_L at small scales ($r/\eta < 2$).

Third, as shown in the inset of Fig. 4(b), the inter-particle coherency decreases with Sv_L , and the droplet motions in gravity direction are more coherent than those in the horizontal direction, i.e., $\rho_{22} > \rho_{11}$; this has also been observed in particle-laden vertical channel flow.⁵ This can be explained as follows. The rapid settling of droplets can hinder particle–turbulence interactions. As shown in Table III, the time taken for drops to pass through the turbulence box decreases with Sv_L ; that is, for larger Sv_L values, the droplets have less time to interact with the turbulent flows, and they, thus, possess less coherency. In addition, due to the preferential sweeping effect of the turbulent structures moving downward, the droplets prefer to accumulate in this flow region and tend to fall together.^{46,51} As a result, the vertically settling droplets are more responsive to gravity-direction turbulent fluctuations than to horizontal ones.³³ Thus, the gravity-direction droplet motion can be correlated over longer distances than the horizontal droplet motion. Indeed, for large separations ($r/\eta > 30$), it can be seen in Fig. 4 that for droplets, the ρ_{22} values are noticeably larger than the ρ_{11} values.

Figure 5 shows radial two-dimensional kinetic energy spectra of the two velocity components of both the droplet and fluid phases for all cases. These were obtained by performing a Fourier transform of the two-point correlation (see Fig. 4) using a Hann window. In the large-scale (low-wavenumber) range, the fluid-phase energy spectra present the classical Kolmogorov $-5/3$ power law for both velocity

components. Conversely, in the high-wavenumber (small-scale) range, the energy spectra deviate from this power-law decay, which has also been reported in previous studies.^{36,37} This deviation may be attributed to measurement uncertainty and the small-scale information suffering more from the signal noise.

For the droplet phase, it is worth noting that the energy spectra essentially reflect the energy distribution of the droplet motion under the action of turbulent structures of different scales. In the small- and large-scale ranges, the kinetic energy of the u_{p2} component is found to be higher than that of the u_{p1} component, which is consistent with the anisotropic behavior of droplet motion ($u_{p1,rms} < u_{p2,rms}$). Aside from a small difference in energy magnitude, the energy spectra in the two directions for different Sv_L values present almost the same behavior. In the large-scale range, although the kinetic energy of the droplets is slightly lower than that of fluid phase (i.e., $u_{p,rms} < u_{f,rms}$), the energy spectra for the droplet phase also approximately present a $-5/3$ power law. This observation indicates the significant role of the inertial-range turbulent structures on the large-scale droplet kinematics.

Surprisingly, in the small-scale range, the energy distribution of the droplet motion is distinctly different from that of the fluid phase. On the one hand, the small-scale droplet motions have more kinetic energy than the turbulence, which can be attributed to inertial effects. On the other hand, the droplet motions are inclined to have nearly the same energy near the dissipation range ($k_r \gtrsim 1000 \text{ m}^{-1}$, $k_r\eta \gtrsim 0.2$ or

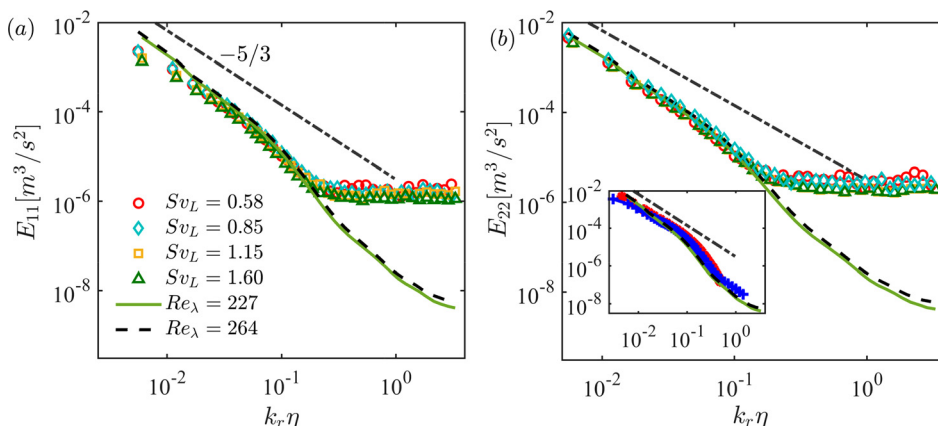


FIG. 5. Two-dimensional kinetic-energy spectra for the two phases: (a) u_1 component; (b) u_2 component. In the inset of (b), the energy spectra of HIT reported by Gotoha *et al.*⁴⁸ ($Re_{zi} = 284$, red symbols) and de Jong *et al.*⁴⁹ ($Re_{zi} = 181$, blue symbols) are shown for comparison.

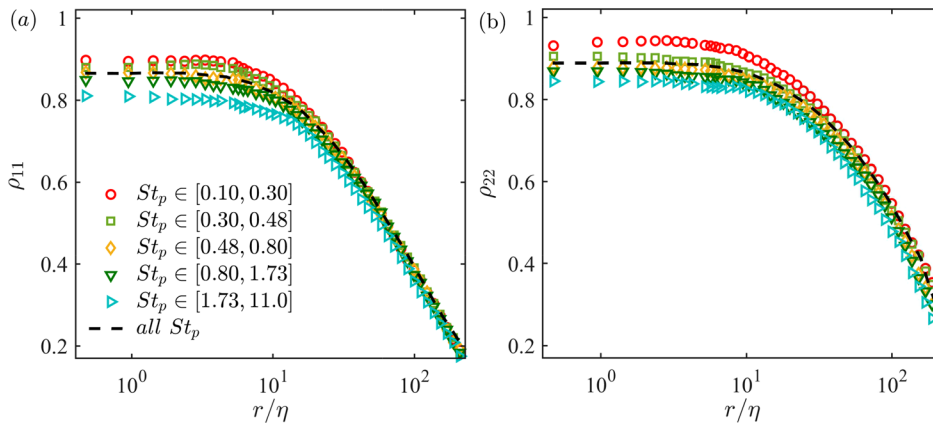


FIG. 6. Conditional SVCs of droplet phase ($Sv_L = 0.58$) for different ranges of St_p : (a) ρ_{11} ; (b) ρ_{22} . The unconditional results (all St_p) are also shown as black dashed lines for reference.

$r/\eta < 5$). Specifically, the energy distribution in this range presents nearly scale-invariant behavior. We believe that this behavior may have a twofold explanation. First, the particle–particle interactions near the dissipation range have recently been found to distinctly enhance the particle clustering.^{27,28} These interactions (including particle collisions and hydrodynamic interactions) may cause the kinetic energy of droplets to be uniformly transferred to different small scales. Second, the present settling parameter Sv_η is greater than 6 (see Table III); specifically, the particle settling velocity is at least six times greater than the Kolmogorov velocity of the turbulence. Thus, considering the effect of the finite size and rapid settling of the droplets, the turbulent motions near the dissipation range have a relatively limited impact on their kinetic energy. This is also consistent with previous studies in which it was demonstrated that the particle trajectories in the small-scale range are nearly ballistic due to inertial effects.¹⁸ Nevertheless, small-scale turbulence indeed plays a role in the particle RVs in the dissipation range through the so-called path-history mechanism, as mentioned above.^{18,24,25,50} This will be discussed in Sec. IV.

We now consider the effects of St_p on droplet SVCs. Figure 6 shows plots of the conditional SVCs (ρ_{ii}) in different ranges of St_p . It is seen that at small separations, the magnitudes of the SVCs decrease with the increase in St_p for both velocity components. Physically, this feature suggests that the trajectories of neighboring high-inertia particles become more independent. This trend becomes weak at large scales, which is consistent with the DNS results of F evrier *et al.*,⁴ although a clear St_p dependence of ρ_{22} can still be seen.

IV. DROPLET RV

The statistics of developed turbulence are commonly investigated by means of the velocity increments (or RVs) between two points with a separation of r , i.e., $\delta u_i(r) = u_i(x + r) - u_i(x)$, the n -order moments of which are called velocity structure functions, S^n . When the separation r is parallel to u , we have the longitudinal components δu_i^L and S^{nL} , while the transverse components δu_i^T and S^{nT} are obtained if r is perpendicular to u . Here, we only consider the longitudinal statistics and will, thus, omit the superscript L .

Figures 7(a) and 7(b) show the probability density functions (PDFs) of δu_1 normalized by $S_{f|p1}^2$ for both the fluid and droplet phases at four typical scales r , ranging from $r/\eta = 150$ (large scale), through 50 (typical inertial scale) and 10 (intermediate scale), down to

1 (close to the dissipative scale). In Figs. 7(c) and 7(d), the PDFs of δu_{p1} and δu_{p2} in different ranges of St_p at $r/\eta = 1$ are shown for $Sv_L = 0.58$. The related results for the u_2 component and the other cases are similar, and these are, thus, omitted for concision. We now consider the statistical measures to quantify the shapes of the PDFs associated with the effects of Sv_L and St_p .

A. Sv_L effect

Figures 8 and 9 show the second-order moment S^2 and the flatness $Ft [= S^4/(S^2)^2]$ of the RVs as functions of r/η , respectively, for all tested cases of both the fluid and droplet phases. It is worth noting that the first-order structure functions S^1 , i.e., the mean RV, have similar qualitative trends to S^2 , as demonstrated by previous studies.^{16,23,25} In addition, here, we do not consider the inward RV (i.e., the RV along the separation vector), which directly contributes to the particle collision rate,^{25,26,28} because we would like to investigate the effects of settling on the small- and large-scale relative motions of droplets by comparing S_{p2}^2 with S_{p1}^2 .

As shown in Fig. 8, both $r^{2/3}$ scaling in the inertial range and r^2 scaling in the dissipative range are observed; these are characteristics of isotropic turbulence.^{11,40} Figures 8(a) and 8(b) also present plots of the S_{pi}^2 of the droplet phase for different Sv_L values. There is a two-branch behavior characterized by a critical scale ($r/\eta \sim 20$) for S_{pi}^2 , and this scale seems to decrease with Sv_L . Specifically, at small separations, S_{pi}^2 is much larger than S_{fi}^2 , and the former changes slowly with r . At larger separations, S_{pi}^2 is slightly smaller than S_{fi}^2 . These observations are consistent with the results of previous DNS studies^{14,18,20} and a few experimental observations.²⁵

The explanation for this two-branch behavior of droplet structure functions may be as follows. At small separations ($r/\eta \lesssim 5$), the small-scale turbulent motions are not energetic enough to affect the droplet motion. Due to the path-history mechanism, the inertia of the droplets enhances the relative particle motion at small separations by causing the particle trajectories to be nearly ballistic.^{18,24,50} Through a Lagrangian description, Gibert *et al.*⁵² found that heavy inertial particles separated faster at small distances than the fluid tracers. This can be confirmed by the correlation functions being remarkably smaller than 1.0 near $r/\eta = 0$, as shown in Fig. 4. At larger separations, large-scale turbulent structures can have an impact on the droplet motion, as shown in Fig. 5. However, inertial effects make the finite-sized

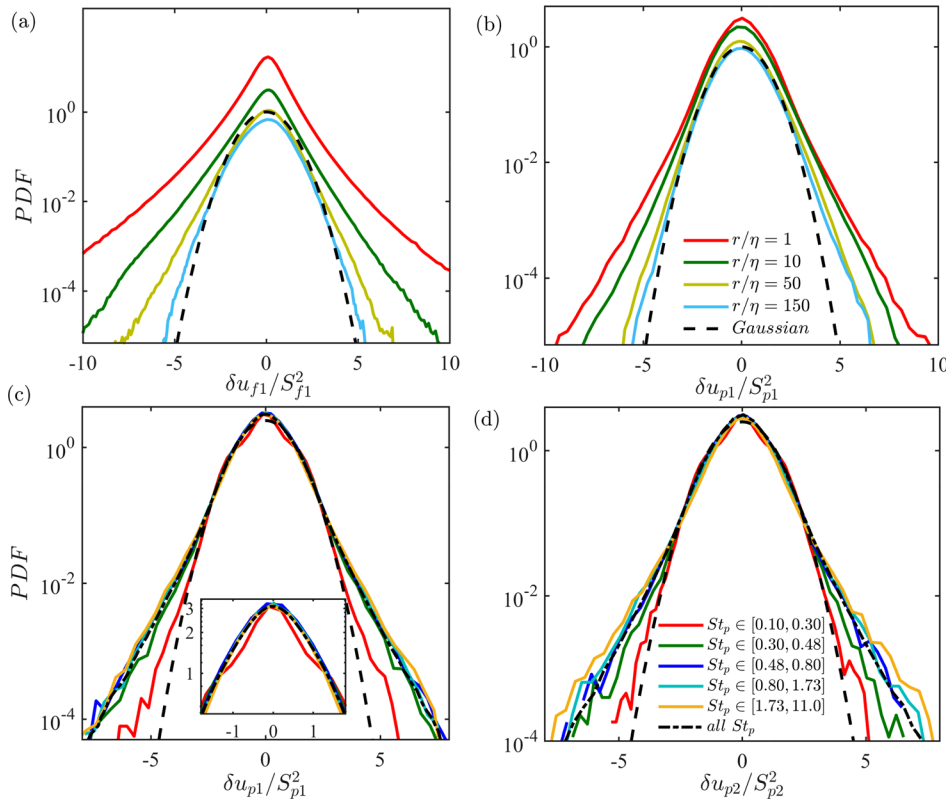


FIG. 7. PDFs of longitudinal velocity increments of fluid and droplet phases at different scales: (a) δu_{f1} ($Re_\lambda = 264$); (b) δu_{p1} ($Sv_L = 0.58$); (c) δu_{p1} ; and (d) δu_{p2} in different ranges of St_p at $r/\eta = 1$ for $Sv_L = 0.58$. The inset of (c) is a zoomed-in section of the main plot to show more clearly the core region of the PDF for $St_p = 0.1-0.3$; this core region also exists for δu_{p2} in (d). The unconditional results (dash-dotted lines) for all St_p are also shown in (c) and (d). The black dashed lines denote a standard Gaussian distribution.

droplets “filter” the strong turbulent fluctuations, and thus, their RVs are lower than those of the turbulence, which is called the inertial filtering mechanism.^{16,22,25} We can see that at large separations, S_{p2}^2 decreases with Sv_L and is larger than S_{p1}^2 . This is because the correlation time of droplet motion with turbulent flows in the direction of gravity is larger than that in the horizontal direction, as mentioned in Sec. III. Moreover, as shown in Figs. 10 and 11, S_{pi}^2 decreases with St_p at large separations, which is also consistent with the picture above.

The deviation of the PDF profiles from a standard Gaussian is usually characterized as intermittency, and this is measured by flatness. In

Fig. 9, we can see that above the dissipation range, the flatness of both phases $Ft_{f|p}$ decreases slowly with scale and approaches 3.0 in the large scale, which is consistent with the results shown in Fig. 7. This observation agrees with the results of previous studies of single- and two-phase turbulent flows.^{11,23,24} Moreover, at a given scale, the turbulent flow presents higher intermittency than the droplet motion, which can also be observed from the more pronounced tails of the PDFs for the fluid phase in Fig. 7. Although this result is inconsistent with the results of numerical simulations that ignore gravity,^{14,16,20} the inclusion of gravity has indeed been found to decrease the intermittency of inertial particles.^{22,29}

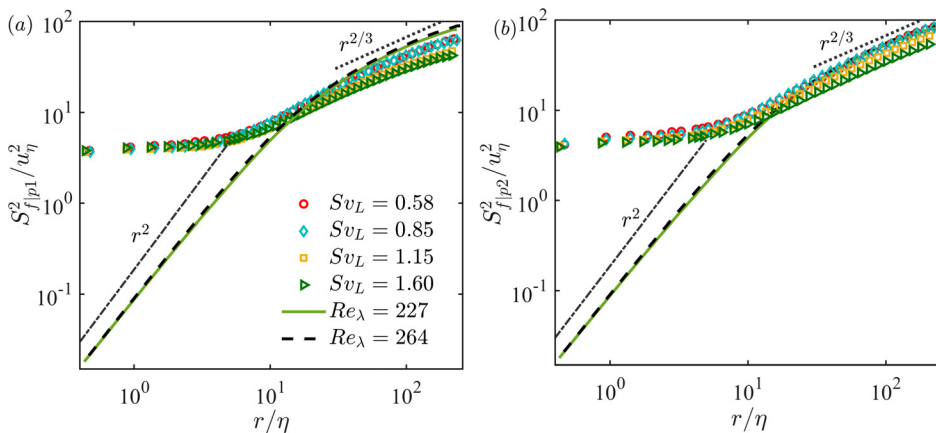


FIG. 8. Second-order structure functions of the (a) u_1 and (b) u_2 components for both the fluid and droplet phases. Both $r^{2/3}$ scaling in the inertial range and r^2 scaling in the dissipative range are also shown.

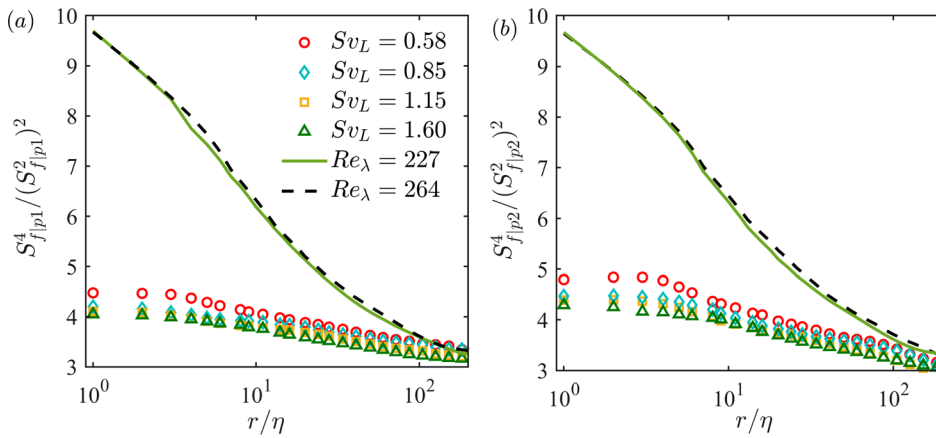


FIG. 9. Flatness of the longitudinal velocity increments of the two phases as functions of r/η : (a) u_1 component; (b) u_2 component.

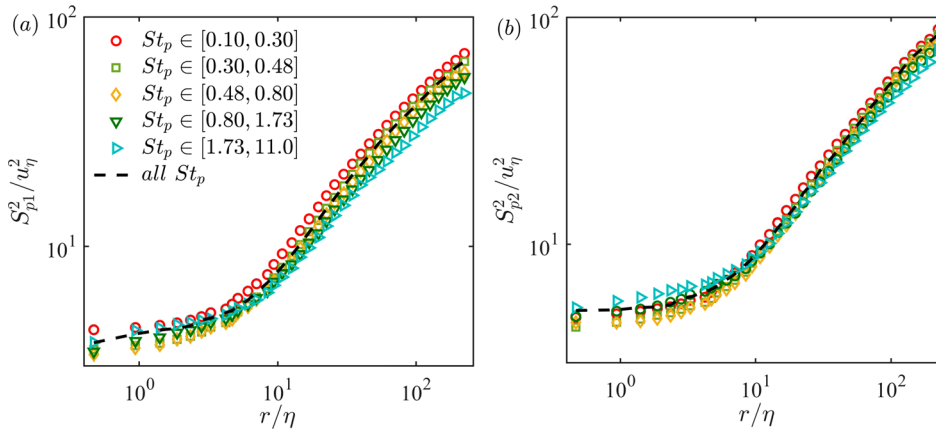


FIG. 10. Second-order structure functions of the (a) u_{p1} and (b) u_{p2} components in different ranges of St_p for $Sv_L = 0.58$. The unconditional result for all St_p is also shown by the black dashed line.

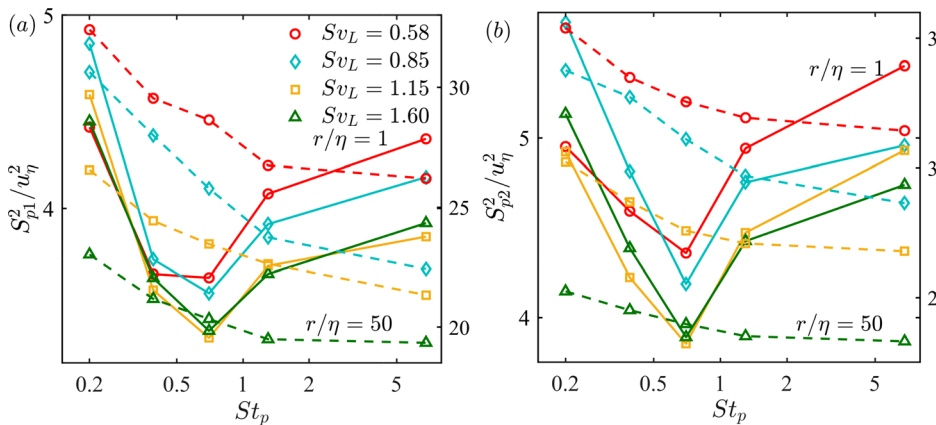


FIG. 11. Second-order structure functions of (a) u_{p1} and (b) u_{p2} components as functions of St_p at $r/\eta = 1$ (solid lines, left ordinate) and $r/\eta = 50$ (dashed lines, right ordinate) for different Sv_L values.

Below the large-scale range ($r/\eta < 100$), Ft_{p2} is found to be noticeably larger than Ft_{p1} , indicating the higher intermittency for the gravity-direction velocity increments. In addition, we found that Ft_p decreases with Sv_L . As observed in Fig. 4, the droplet motions are correlated over longer distances in the gravity direction than in the

horizontal direction. This is because the vertically settling droplets are more responsive to the gravity-direction turbulent motions. Therefore, the settling velocities of droplets fluctuate more intensely and have stronger intermittency. Similarly, as Sv_L increases, in the settling regime, the correlation time (see Table III) of the droplet motion with

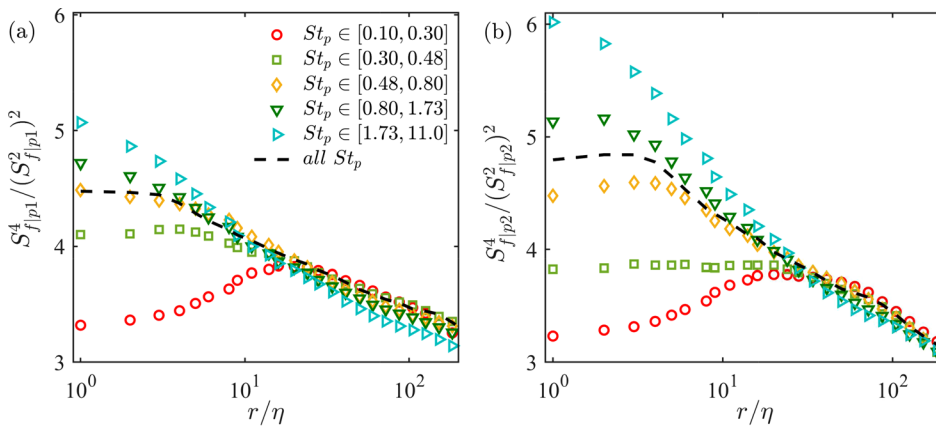


FIG. 12. Flatness of droplet RVs ($Sv_L = 0.58$) as functions of r/η for different ranges of St_p : (a) u_1 component; (b) u_2 component.

the turbulent fluctuations decreases, resulting in decreasing intermittency of droplet motion.²⁹ It is interesting that near the dissipation range ($r/\eta < 5$), Ft_p is nearly independent of separation. This scale invariance of intermittency (and energy distribution in Fig. 5) will be discussed below.

B. St_p effect

Figure 10 shows S^2_{pi} as functions of r/η in different ranges of St_p for $Sv_L = 0.58$, and Fig. 11 presents the St_p dependence of S^2_{pi} at $r/\eta = 1$ and $r/\eta = 50$ for four cases of Sv_L . Interestingly, we found that for small separations, the droplet RVs in two directions present a non-monotonic trend with separation r , and they reach their minimum at $St_p \approx 0.7$, as shown in Fig. 11. This observation seems to be inconsistent with the results of previous DNS studies^{18,20} in which it was demonstrated that, for small separations, the larger the value of St_p , the larger the value of S^2_{pi} . Dou *et al.*²⁵ suggested from their experiments that the particle RV increases slowly with St_p , although their data seem to be relatively scattered for $St_p \gtrsim 1.0$ and they did not consider the effects of settling. However, using DNS, Ireland *et al.*²² found that for a small settling parameter (e.g., $Sv_\eta < 10$), S^2_{pi} increases with St_p , while for large Sv_η (>10), a non-monotonic trend was observed, and the smallest value occurred for $St_p \sim 1.0$. In the present work, the

settling parameter Sv_η for all cases ranged from 6.8 to 17.6 (see Table III). The present results do not, therefore, seem to contradict the observations of Ireland *et al.*²² The physical explanation for this non-monotonic behavior is as follows.

First, the path-history effect, which contributes to increasing RV, is more significant for larger St_p , as shown in Fig. 11. Second, preferential concentration, which leads to particle clustering, is known to be strongest for an St_p value of unity.^{1,38} Inside a particle cluster, the particles are expected to share a similar velocity (i.e., to have coherent motion⁵¹) and have smaller RVs. Finally, under the effect of settling, the preferential sweeping effect, in which particles prefer to reside in the downward-motion flow field,^{15,46,51} is prevalent at $St_p \sim 1.0$. This can also induce smaller relative motions among particles. Taking these points together, it can be expected that the RVs of settling droplets may reach a minimum at $St_p \sim 1.0$.

Figure 12 shows the flatness of the droplet RVs ($Sv_L = 0.58$) as functions of r/η for different ranges of St_p . The St_p dependences of the flatness at $r/\eta = 1$ and $r/\eta = 50$ for four cases of Sv_L are shown in Fig. 13. Combined with the PDFs in Figs. 7(c) and 7(d), there are two interesting observations that can be made regarding Figs. 12 and 13.

First, for the smallest St_p values (0.1–0.3), a non-monotonic r dependence of the intermittency is observed, and this is different from that for larger St_p values in which Ft_p increases with r for $r/\eta \lesssim 20$

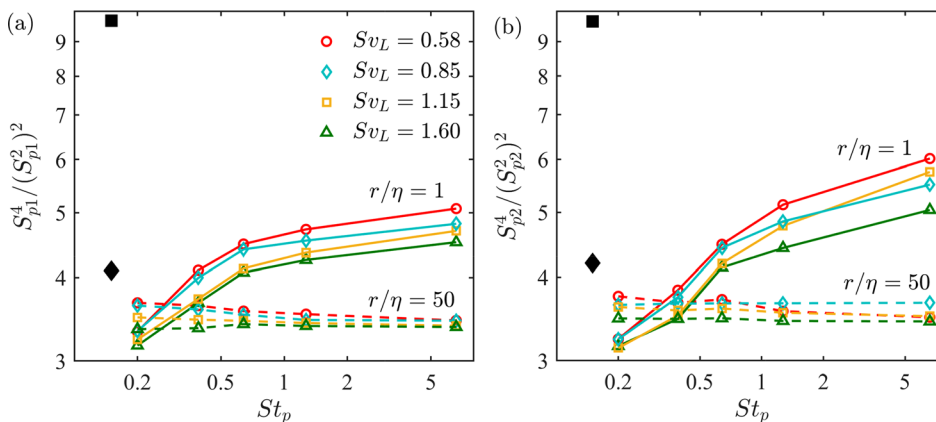


FIG. 13. Flatness of droplet RVs ($Sv_L = 0.58$) as functions of St_p at $r/\eta = 1$ (solid lines) and $r/\eta = 50$ (dashed lines) for different Sv_L values: (a) u_1 component; (b) u_2 component. The black squares and diamond symbols denote the corresponding values of the fluid phase ($Re_\lambda = 227$) for $r/\eta = 1$ and $r/\eta = 50$, respectively.

Downloaded from http://pubs.aip.org/journal/phf/article-pdf/doi/10.1063/5.0101945/16574719/083320_1_online.pdf

and decreases for $r/\eta \gtrsim 20$. This difference can be attributed to the occurrence of core-and-tail behavior in the PDFs of velocity increments with small separations for $St_p = 0.1\text{--}0.3$ [see the inset of Fig. 7(c)]. This phenomenon has also been observed for both velocity components in other cases of Sv_L . In a recent experiment, Hammond and Meng²⁸ also noticed this core-and-tail behavior and found that the core became obscured with increasing r/η , in agreement with the present work. They suggested that there could be two mechanisms driving the particle RV at small separations, but they did not provide further explanation. To our knowledge, the core region of PDF(δu) around $\delta u \approx 0$ with higher probability may originate from the fact that two particles with very close distance are expected to share the same velocity ($\delta u \approx 0$) when $r \lesssim \eta$. In addition, it is seen that this core-and-tail behavior can only be observed for small- St_p ($St_p \lesssim 0.5$) particles, which are more likely to follow the turbulent flows. Nevertheless, the particle-particle interaction may lead to extreme events, i.e., very large RVs. This might explain the occurrence of the long tail in PDF(δu). It is worth noting that the core region observed by Hammond and Meng²⁸ was more pronounced than that seen in these experiments. This may be attributed to their higher-resolution 3D measurements, which were able to resolve near-contact events of particles.

Second, for $r/\eta \lesssim 20$, Ft_p increases with St_p , consistent with the observations in Figs. 7(c) and 7(d), while for $r/\eta \gtrsim 20$, the opposite is observed, as shown in Fig. 13. For large separations, decreasing intermittency with St_p can be expected because the larger the value of St_p , the stronger the inertial filtering of droplets from large-scale turbulent fluctuations. That is, the diminished influence of turbulent motions leads to a reduction of the intermittency of droplet motion. At small separations, Ireland *et al.*²² also found that the intermittency of particles increased with St_p without consideration of gravity; with gravity, a non-monotonic trend of intermittency with St_p was observed. As noted above, the path-history effect becomes more significant with larger values of St_p . Therefore, when St_p is larger, extreme events of the droplet RVs at small separations occur more frequently, leading to greater intermittency. However, the reason that the critical scale r/η is around 20 seems unclear; we note that in Fig. 8, there is also a critical scale ($r/\eta \approx 20$) for the droplet RV. Recall that in addition to the turbulent structures, the path-history effect has an impact on the small-scale RV, while the effect of inertial filtering has an impact on the large-scale RV; furthermore, both effects become stronger with increasing St_p . Therefore, this critical scale could be used to characterize the dominant effects associated with particle inertia on the particle RV, and this can be more noticeably characterized with respect to intermittency.

Finally, we focus on the velocity statistics of droplets near the dissipation range ($r/\eta < 5$). It is found that above the intermediate range of turbulent flows, the SVCs (Fig. 4), energy distributions (Fig. 5), RVs (Fig. 8), and intermittencies (Fig. 9) of droplets vary notably with scale. However, for $r/\eta < 5$, we found that these droplet velocity statistics are almost constant or change only slightly. Note that previous DNS results have also shown a scale-independence of RV near the dissipation range for relatively high St_p values (>1).^{18,20} In this work, this scale-independent behavior was found for not only the RVs but also the energy distribution and intermittency of droplets. On the one hand, as mentioned in Sec. III, at small separations, inter-droplet interactions (particle collisions and hydrodynamic interactions) become stronger, and thus, the droplet motions are independent of scale to a

certain degree. On the other hand, we note that in this range, the correlation coefficient of the turbulent velocity is nearly independent of length scale, while the RVs and energy distribution of turbulence display clear scale dependence. Therefore, near the dissipation range, the turbulent coherent motions seem to play an important role in the scale independence of the velocity statistics of particle motion. Furthermore, the scale independence of intermittency seems to be more pronounced for medium St_p values ($0.3 < St_p < 1.73$, i.e., when the particle response time is comparable to the Kolmogorov timescale of the turbulence) in this work. It can, thus, be concluded that the balance between the path-history effect and turbulent motions may lead the velocity statistics of inertial particles to present nearly scale-independent behavior near the dissipation range.

V. CONCLUSIONS

The motions of polydisperse droplets in HIT were experimentally investigated for Taylor Reynolds numbers in the range $Re_\lambda = 200$ to 300 and particle settling parameters in the range $Sv_L = 0.5$ to 2.0. Thanks to the present high-resolution measurements, we were also able to study the effect of the Kolmogorov timescale-based particle Stokes number St_p ($= 10^{-1}$ to 10^1) by identifying different sizes from the droplet images, and the turbulent and droplet motions could be resolved over a wide scale range ($10^{-1}\eta$ to $10^2\eta$). In this work, the emphasis was placed on the RVs and SVCs of droplets, which are related to the particle collision rates and particle dispersion under the action of turbulent coherent structures. We investigated their Sv_L and St_p dependences, reflecting the importance of settling and particle inertia relative to the effects of turbulent flows on droplet motion.

There is a gap at the origin between the SVCs of droplets and unity, which can be attributed to the effects of particle inertia. More importantly, the SVCs of droplets also present a parabolic form similar to that seen for turbulent flows. These observations indicate that the motions of droplets are inherited from the coherency of small-scale turbulent motions, but due to the effects of inertia, they are less coherent. With increasing Sv_L , both the SVCs and RVs were found to be diminished because the correlation time of droplet motion with turbulent structures is reduced. For the same reason, there are distinct differences in the velocity statistics in the gravity and horizontal directions. Additionally, the correlation time is smaller for higher St_p values; thus, the SVCs and RVs of droplets are found to decrease with St_p in the large-scale range.

Due to particle inertia, the path-history effect in the small-scale range and the inertial filtering effect in the large-scale range lead to the droplet RVs being larger and smaller than those of the turbulent flows, respectively. Furthermore, there is a critical scale ($r/\eta \approx 20$) characterizing the dominant effect associated with particle inertia on droplet motion, and this critical scale seems to be related to both Sv_L and St_p . Below this scale, the path-history effect combined with the action of turbulence structures dominates the particle motion; above this scale, the filtering effect plays a more significant role. More importantly, this critical scale seems to be more noticeably characterized when considering the St_p dependence of the intermittency of droplet motion. Specifically, for $r/\eta \lesssim 20$, Ft_p increases with St_p , while for $r/\eta \gtrsim 20$, the opposite trend is observed.

The RVs of inertial droplets in the small-scale range were found to present a non-monotonic trend with St_p , and they reach a minimum value at $St_p \sim 1.0$. We attribute this behavior to the effect of

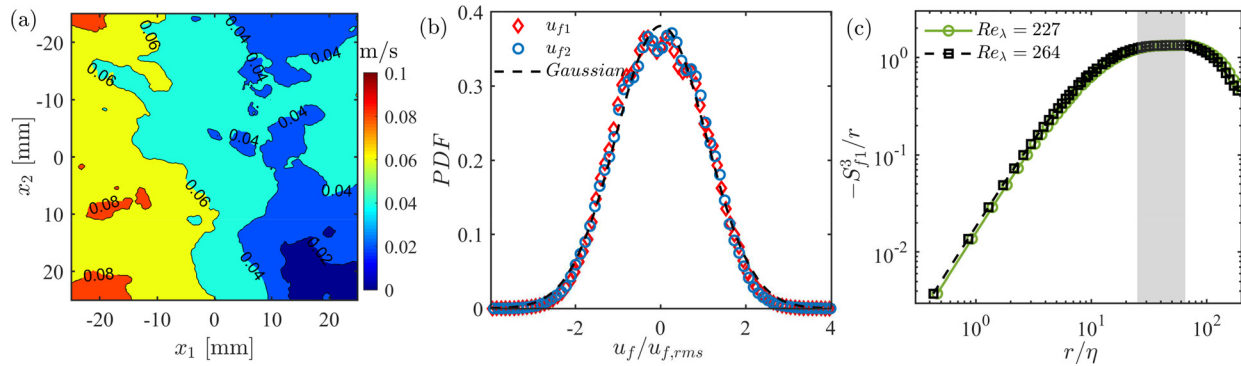


FIG. 14. (a) Time-averaged velocity field $\bar{U} = \sqrt{\bar{u}_1^2 + \bar{u}_2^2}$ for $Re_\lambda = 264$. (b) PDFs of velocity fluctuations in two directions for $Re_\lambda = 264$. (c) Compensated third-order structure functions $S_{f1}^3 = \langle u_1(x+r) - u_1(x) \rangle^3 / u_t^3$ for two Re_λ cases; the shaded region indicates the determined inertial range ($25 \leq r/\eta \leq 70$) for the scaling $S_f^3 \propto r$.

particle clustering and preferential sweeping, because both are prevalent at $St_p \sim 1.0$ and lead the particles to share similar velocities and, thus, have small RVs. Furthermore, near the dissipation range ($r/\eta < 5$), the balance between the path-history effect due to particle inertia and the action of turbulent coherent motions leads the velocity statistics of inertial particles, including the SVCs, energy distributions, and particle RVs and their intermittency, to present nearly scale-independent behavior. Finally, core-and-tail behavior in the PDFs of droplet RVs with small separations for small St_p was observed. We found that this behavior has a significant impact on the scale variance of the intermittency.

In summary, the present work explores the effect of St_p and Sv_L on particle motions in HIT, which could facilitate the understanding of particle transport and dispersion in turbulence. Specifically, the St_p dependence of particle RVs observed in the present work is of importance for modeling particle collision rates in turbulence. Recalling that particle collision rate is not only related to the RVs but also related to the effect of particle clustering. To fully address the issues of particle collisions, particle clustering under the action of turbulent structures is needed to be studied in the future.

ACKNOWLEDGMENTS

Hang-Yu Zhu is currently a postdoctoral fellow at SUSTech. This work was a joint Ph.D. research program between Institute of Mechanics (Chinese Academy of Sciences) and Beihang University. Hang-Yu Zhu greatly appreciates the assistance of Tuo Li and Rui-Xu Zhou in the experiments. This work was supported by the National Natural Science Foundation of China (NSFC) (Grant Nos. 91941104 and 11872366).

AUTHOR DECLARATIONS

Conflict of Interest

The authors have no conflicts to disclose.

Author Contributions

Hangyu Zhu: Data curation (lead); Formal analysis (lead); Methodology (equal); Writing – original draft (equal); Writing – review and editing (equal). **Chong Pan:** Conceptualization (equal);

Data curation (equal); Formal analysis (supporting); Methodology (supporting); Writing – original draft (equal); Writing – review and editing (equal). **Huan Lian:** Conceptualization (equal); Data curation (equal); Funding acquisition (lead); Methodology (equal); Project administration (lead); Writing – original draft (equal); Writing – review and editing (equal).

DATA AVAILABILITY

The data that support the findings of this study are available from the corresponding author upon reasonable request.

APPENDIX: VERIFICATION OF THE HOMOGENEOUS AND ISOTROPIC CONDITIONS

The results shown in Fig. 14 provide a verification of the homogeneity and isotropy of the turbulent flows in the present experiments.

REFERENCES

- ¹S. Balachandar and J. K. Eaton, “Turbulent dispersed multiphase flow,” *Annu. Rev. Fluid Mech.* **42**, 111–133 (2010).
- ²G. A. Voth and A. Soldati, “Anisotropic particles in turbulence,” *Annu. Rev. Fluid Mech.* **49**(1), 249–276 (2017).
- ³L. Brandt and F. Coletti, “Particle-laden turbulence: Progress and perspectives,” *Annu. Rev. Fluid Mech.* **54**, 159–189 (2022).
- ⁴P. Février, O. Simonin, and K. D. Squires, “Partitioning of particle velocities in gas–solid turbulent flows into a continuous field and a spatially uncorrelated random distribution: Theoretical formalism and numerical study,” *J. Fluid Mech.* **533**, 1–46 (2005).
- ⁵K. O. Fong, O. Amili, and F. Coletti, “Velocity and spatial distribution of inertial particles in a turbulent channel flow,” *J. Fluid Mech.* **872**, 367–406 (2019).
- ⁶M. W. Vance, K. D. Squires, and O. Simonin, “Properties of the particle velocity field in gas–solid turbulent channel flow,” *Phys. Fluids* **18**(6), 063302 (2006).
- ⁷E. Meneguz and M. W. Reeks, “Statistical properties of particle segregation in homogeneous isotropic turbulence,” *J. Fluid Mech.* **686**, 338–351 (2011).
- ⁸D. A. Khalitov and E. K. Longmire, “Effect of particle size on velocity correlations in turbulent channel flow,” in *4th ASME/JSME Joint Fluids Summer Engineering Conference, Hawaii* (American Society of Mechanical Engineers, 2003).
- ⁹S. Sahu, Y. Hardalupas, and A. M. Taylor, “Droplet-turbulence interaction in a confined polydispersed spray: Effect of droplet size and flow length scales on spatial droplet-gas velocity correlations,” *J. Fluid Mech.* **741**, 98–138 (2014).

Downloaded from http://pubs.aip.org/aip/pof/article-pdf/doi/10.1063/5.0101945/16574719/083320_1_online.pdf

- ¹⁰L. I. Zaichik and V. M. Alipchenkov, "Pair dispersion and preferential concentration of particles in isotropic turbulence," *Phys. Fluids* **15**, 1776–1787 (2003).
- ¹¹U. Frisch, *Turbulence: The Legacy of A.N. Kolmogorov* (Cambridge University Press, 1995).
- ¹²L. P. Wang, A. S. Wexler, and Y. Zhou, "Statistical mechanical description and modelling of turbulent collision of inertial particles," *J. Fluid Mech.* **415**, 117–153 (2000).
- ¹³M. Hirschler, G. Oger, U. Niekien, and D. Le Touzé, "Modeling of droplet collisions using smoothed particle hydrodynamics," *Int. J. Multiphase Flow* **95**, 175–187 (2017).
- ¹⁴J. Bec, L. Biferale, M. Cencini, A. S. Lanotte, and F. Toschi, "Intermittency in the velocity distribution of heavy particles in turbulence," *J. Fluid Mech.* **646**, 527–536 (2010).
- ¹⁵M. R. Maxey, "The gravitational settling of aerosol particles in homogeneous turbulence and random flow fields," *J. Fluid Mech.* **174**, 441–465 (1987).
- ¹⁶P. J. Ireland, A. D. Bragg, and L. R. Collins, "The effect of Reynolds number on inertial particle dynamics in isotropic turbulence. Part 1. Simulations without gravitational effects," *J. Fluid Mech.* **796**, 617–658 (2016).
- ¹⁷G. Falkovich and A. Pumir, "Sling effect in collisions of water droplets in turbulent clouds," *J. Atmos. Sci.* **64**, 4497–4505 (2007).
- ¹⁸A. D. Bragg and L. R. Collins, "New insights from comparing statistical theories for inertial particles in turbulence: II. Relative velocities," *New J. Phys.* **16**, 055014 (2014).
- ¹⁹J. P. L. C. Salazar and L. R. Collins, "Inertial particle acceleration statistics in turbulence: Effects of filtering, biased sampling, and flow topology," *Phys. Fluids* **24**(8), 083302 (2012).
- ²⁰J. P. L. C. Salazar and L. R. Collins, "Inertial particle relative velocity statistics in homogeneous isotropic turbulence," *J. Fluid Mech.* **696**, 45–66 (2012).
- ²¹S. Ayyalasomayajula, Z. Warhaft, and L. R. Collins, "Modeling inertial particle acceleration statistics in isotropic turbulence," *Phys. Fluids* **20**(9), 095104 (2008).
- ²²P. J. Ireland, A. D. Bragg, and L. R. Collins, "The effect of Reynolds number on inertial particle dynamics in isotropic turbulence. Part 2. Simulations with gravitational effects," *J. Fluid Mech.* **796**, 659–711 (2016).
- ²³L. Pan and P. Padoan, "Turbulence-induced relative velocity of dust particles. I. Identical particles," *Astrophys. J.* **776**, 12 (2013).
- ²⁴E. Saw, G. P. Bewley, E. Bodenschatz, S. S. Ray, and J. Bec, "Extreme fluctuations of the relative velocities between droplets in turbulent airflow," *Phys. Fluids* **26**(11), 111702 (2014).
- ²⁵Z. Dou, A. D. Bragg, A. L. Hammond, Z. Liang, L. R. Collins, and H. Meng, "Effects of Reynolds number and Stokes number on particle-pair relative velocity in isotropic turbulence: A systematic experimental study," *J. Fluid Mech.* **839**, 271–292 (2018).
- ²⁶A. D. Bragg, A. L. Hammond, R. Dhariwal, and H. Meng, "Hydrodynamic interactions and extreme particle clustering in turbulence," *J. Fluid Mech.* **933**, A31 (2022).
- ²⁷M. A. Yavuz, R. P. J. Kunnen, G. J. F. Van Heijst, and H. J. H. Clercx, "Extreme small-scale clustering of droplets in turbulence driven by hydrodynamic interactions," *Phys. Rev. Lett.* **120**(24), 244504 (2018).
- ²⁸A. Hammond and H. Meng, "Particle radial distribution function and relative velocity measurement in turbulence at small particle-pair separations," *J. Fluid Mech.* **921**, A16 (2021).
- ²⁹H. Parishani, O. Ayala, B. Rosa, L. P. Wang, and W. W. Grabowski, "Effects of gravity on the acceleration and pair statistics of inertial particles in homogeneous isotropic turbulence," *Phys. Fluids* **27**(3), 033304 (2015).
- ³⁰P. S. Goswami and V. Kumaran, "Particle dynamics in the channel flow of a turbulent particle-gas suspension at high Stokes number. Part 2. Comparison of fluctuating force simulations and experiments," *J. Fluid Mech.* **687**, 41–71 (2011).
- ³¹Z. Dou, P. J. Ireland, A. D. Bragg, Z. Liang, L. R. Collins, and H. Meng, "Particle-pair relative velocity measurement in high-Reynolds-number homogeneous and isotropic turbulence using 4-frame particle tracking velocimetry," *Exp. Fluids* **59**, 30 (2018).
- ³²J. Bec, H. Homann, and S. S. Ray, "Gravity-driven enhancement of heavy particle clustering in turbulent flow," *Phys. Rev. Lett.* **112**, 184501 (2014).
- ³³G. H. Good, P. J. Ireland, G. P. Bewley, E. Bodenschatz, L. R. Collins, and Z. Warhaft, "Settling regimes of inertial particles in isotropic turbulence," *J. Fluid Mech.* **759**, R3 (2014).
- ³⁴M. Momenifar, R. Dhariwal, and A. D. Bragg, "Influence of Reynolds number on the motion of settling, bidisperse inertial particles in turbulence," *Phys. Rev. Fluids* **4**(5), 054301 (2019).
- ³⁵B. Arcen, R. Ouchene, M. Khalij, and A. Tanière, "Prolate spheroidal particles' behavior in a vertical wall-bounded turbulent flow," *Phys. Fluids* **29**(9), 093301 (2017).
- ³⁶W. Hwang and J. K. Eaton, "Creating homogeneous and isotropic turbulence without a mean flow," *Exp. Fluids* **36**, 444–454 (2004).
- ³⁷C. Goepfert, J.-L. Marié, D. Chareyron, and M. Lance, "Characterization of a system generating a homogeneous isotropic turbulence field by free synthetic jets," *Exp. Fluids* **48**, 809–822 (2010).
- ³⁸H. Lian, G. Charalampous, and Y. Hardalupas, "Preferential concentration of poly-dispersed droplets in stationary isotropic turbulence," *Exp. Fluids* **54**(5), 1525 (2013).
- ³⁹S. B. Pope, *Turbulent Flows* (Cambridge University Press, 2000).
- ⁴⁰D. Carter, A. Petersen, O. Amili, and F. Coletti, "Generating and controlling homogeneous air turbulence using random jet arrays," *Exp. Fluids* **57**, 189 (2016).
- ⁴¹S. Elghobashi, "On predicting particle-laden turbulent flows," *Appl. Sci. Res.* **52**, 309–329 (1994).
- ⁴²S. Sumbekova, A. Cartellier, A. Aliseda, and M. Bourgoin, "Preferential concentration of inertial sub-Kolmogorov particles: The roles of mass loading of particles, Stokes numbers, and Reynolds numbers," *Phys. Rev. Fluids* **2**(2), 024302 (2017).
- ⁴³H. Lian, X. Y. Chang, and Y. Hardalupas, "Time resolved measurements of droplet preferential concentration in homogeneous isotropic turbulence without mean flow," *Phys. Fluids* **31**(2), 025103 (2019).
- ⁴⁴R. Clift, J. R. Grace, and M. E. Weber, *Bubbles, Drops, and Particles* (Dover, 2005).
- ⁴⁵C. Crowe, M. Sommerfeld, Y. Tsuji *et al.*, *Multiphase Flows with Droplets and Particles* (CRC Press, 1998).
- ⁴⁶A. J. Petersen, L. Baker, and F. Coletti, "Experimental study of inertial particles clustering and settling in homogeneous turbulence," *J. Fluid Mech.* **864**, 925–970 (2019).
- ⁴⁷H. Y. Zhu, C. Pan, J. J. Wang, Y. R. Liang, and X. C. Ji, "Sand-turbulence interaction in a high-Reynolds-number turbulent boundary layer under net sedimentation conditions," *Int. J. Multiphase Flow* **119**, 56–71 (2019).
- ⁴⁸T. Gotoha, D. Fukayama, and T. Nakano, "Velocity field statistics in homogeneous steady turbulence obtained using a high-resolution direct numerical simulation," *Phys. Fluids* **14**, 1065–1081 (2002).
- ⁴⁹J. de Jong, L. Cao, S. H. Woodward, J. P. L. C. Salazar, L. R. Collins, and H. Meng, "Dissipation rate estimation from PIV in zero-mean isotropic turbulence," *Exp. Fluids* **46**(3), 499–515 (2009).
- ⁵⁰A. D. Bragg, P. J. Ireland, and L. R. Collins, "On the relationship between the non-local clustering mechanism and preferential concentration," *J. Fluid Mech.* **780**, 327–343 (2015).
- ⁵¹L. Baker, A. Frankel, A. Mani, and F. Coletti, "Coherent clusters of inertial particles in homogeneous turbulence," *J. Fluid Mech.* **833**, 364–398 (2017).
- ⁵²M. Gibert, H. Xu, and E. Bodenschatz, "Inertial effects on two-particle relative dispersion in turbulent flows," *Europhys. Lett.* **90**, 64005 (2010).